

# Extreme response of Weyl-Kondo semimetal to Zeeman coupling

Sarah E. Greife,<sup>1,2,\*</sup> Hsin-Hua Lai,<sup>1</sup> Silke Paschen,<sup>3,1</sup> and Qimiao Si<sup>1</sup>

<sup>1</sup>*Department of Physics and Astronomy and Rice Center for Quantum Materials, Rice University, Houston, Texas 77005, USA*

<sup>2</sup>*Theoretical Division, Los Alamos National Laboratory, Los Alamos, New Mexico 87545, USA*

<sup>3</sup>*Institute of Solid State Physics, Vienna University of Technology, 1040 Vienna, Austria*

(Dated: May 16, 2022)

There is considerable interest in the intersection of correlations and topology, especially in metallic systems. Recent theoretical and experimental studies have found that the Kondo effect can drive the emergence of Weyl nodes near the Fermi energy, leading to a Weyl-Kondo semimetal. Here we study the effect of a Zeeman coupling in a nonsymmorphic and noncentrosymmetric Kondo-lattice model. The Kondo-driven Weyl nodes are found to show an extreme response to the tuning of a magnetic field. We find several topologically distinct semimetal regimes, and a phase transition to a Kondo insulator. Our results reveal a key feature for understanding the recent high magnetic-field experiments in a Weyl-Kondo semimetal compound [S. Dzaber et al., arXiv:1906.01182]. Overall implications for strongly correlated topological metals are discussed.

Keywords: Strongly correlated topological phases, heavy-fermion systems, Kondo effect, Weyl semimetal, topological phases, quantum phase transitions

**Introduction:** Strong correlations drive a variety of quantum states of matter [1, 2]. A large Coulomb repulsion often produces local moments that form a part of the building blocks of the low-energy physics. The quantum entanglement between the local moments determines the nature of the ground state. In the presence of itinerant electrons, as in heavy fermion metals, there is also quantum entanglement between the local moments and conduction electrons. The latter gives rise to the celebrated Kondo effect [3] and a rich landscape of metallic quantum phases and quantum critical points [4, 5]. When spin-orbit coupling is also strong, topological metallic states may also appear in the phase diagram. Recent theoretical [6, 7] and experimental [8, 9] studies have shown that the Kondo effect can drive the emergence of Weyl nodes near the Fermi energy, leading to the notion of a Weyl-Kondo semimetal (WKSM). This development provides a new opportunity to utilize the insights about the strong correlation physics of the heavy fermion metals and elucidate how strong correlations and topology intersect in metallic systems.

Strong correlations *per se* amplify a system's response to external stimuli. For example, heavy fermion metals have orders-of-magnitude enhancement in both their thermodynamic properties (*e.g.*, Sommerfeld coefficient, the  $T$ -linear coefficient of the specific heat) and transport quantities (*e.g.*, the  $T^2$  coefficient of the electrical resistivity). In this vein, they have long been explored by a magnetic field, which is a non-thermal tuning parameter and its relatively small variation can trigger phase transitions or help access quantum critical points by perturbing the  $4f$  local moments [10]. This is highlighted by the usage of a magnetic field to reveal a jump in the normal Hall effect that originates from an abrupt change in the Fermi surface at a local quantum critical point [11–19].

More recently, a magnetic field study was carried out on the WKSM compound  $\text{Ce}_3\text{Bi}_4\text{Pd}_3$  [20]. An analysis of the Hall effect, resistivity, and torque magnetometry gives evidence for a magnetic field-tuned two stage transition: a phase transition into a Kondo insulator (KI) phase, and through a second (possibly quantum critical) point into a partially-polarized heavy

Fermi-liquid metal phase.

In this *Letter*, we study the effect of a Zeeman coupling in a nonsymmorphic and noncentrosymmetric Kondo lattice model. We find that the combined time-reversal and inversion symmetry breaking associated with the Zeeman field and a staggered potential produces a progression of topological Lifshitz transitions. The Weyl nodes are annihilated at a Zeeman energy that is smaller than the Kondo energy scale, implying that the strongly correlated topological semimetal retains its heavy fermion character under the magnetic field before it is quenched into a KI. The complete node annihilation happens at a modest (laboratory-accessible) field. This captures an extreme response of the system to the Zeeman coupling, and is to be contrasted with the case of weakly correlated Weyl semimetals whose node annihilation would typically require an orders-of-magnitude larger magnetic field. Our result reveals a key feature for understanding the experiments on  $\text{Ce}_3\text{Bi}_4\text{Pd}_3$  [20].

**Model and Methods:** We begin with a diamond crystal structure, and use the Anderson lattice model,  $\mathcal{H} = \mathcal{H}_c + \mathcal{H}_{cd} + \mathcal{H}_d$  [6, 7], to consider the strong coupling (Kondo) limit. The conduction electrons corresponding to the *spd*-orbitals of heavy fermion systems are represented by a Hamiltonian based on the Fu-Kane-Mele model [21–23],

$$\begin{aligned} \mathcal{H}_c = & t \sum_{\langle ij \rangle, \sigma} \left( c_{i\sigma}^\dagger c_{j\sigma} + \text{H.c.} \right) + \sum_{i, \sigma} \left( m(-1)^i - \mu \right) n_{i\sigma}^c \\ & + i\lambda \sum_{\langle\langle ij \rangle\rangle} \left[ c_{i\sigma}^\dagger (\boldsymbol{\sigma} \cdot \mathbf{e}_{ij}) c_{j\sigma} - \text{H.c.} \right], \end{aligned} \quad (1)$$

with nearest-neighbor ( $\langle i, j \rangle$ ) hopping, chemical potential  $\mu$ , a Dresselhaus-type spin orbit coupling  $\lambda$ , and an inversion symmetry-breaking onsite potential,  $m$ . The electrons are coupled to the  $d$  fermion species (representing the physical  $4f$  moments) through the hybridization term

$$\mathcal{H}_{cd} = V \sum_{i, \sigma} \left( d_{i\sigma}^\dagger c_{i\sigma} + \text{H.c.} \right). \quad (2)$$

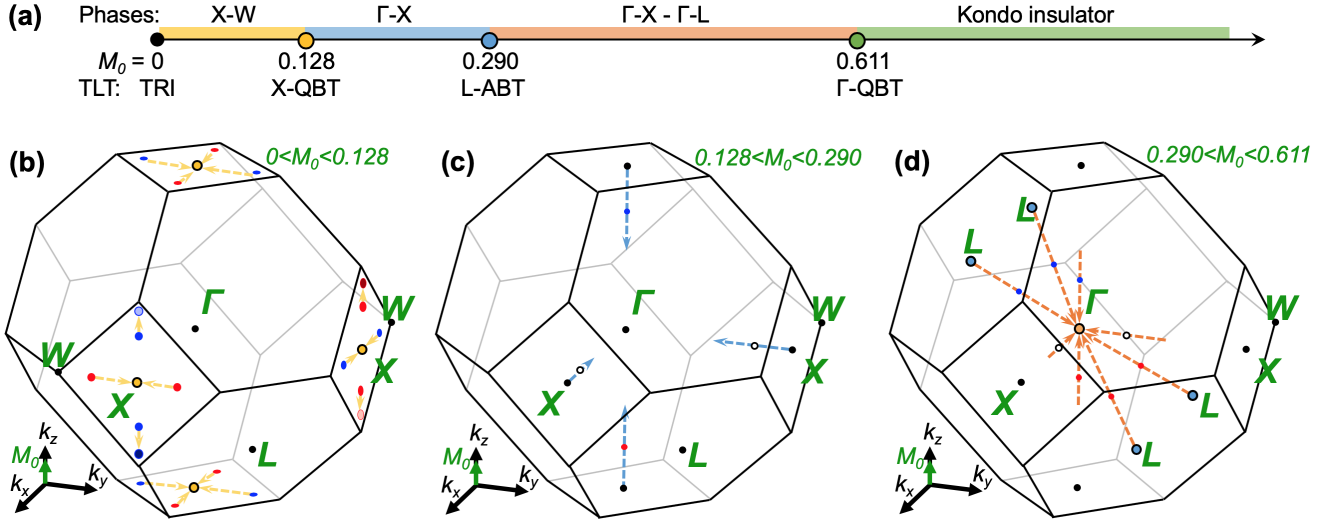


FIG. 1. (a) Phase diagram of the WKSM model as a function of the Zeeman field normalized by the zero-field Kondo temperature,  $M_0 = M_z/T_K^0$ . “Phases” labels where the nodes appear in the BZ for each WKSM regime. “TLT”=topological Lifshitz transition, which classifies the degeneracy and dispersion types involved in each regime crossover at the BZ point. TRI=time-reversal invariant, QBT=quadratic band touching, ABT=anisotropic band touching. (b)-(d) show the path of selected nodes through the fcc BZ for each WKSM regime, where red (blue) refers to  $-1$  ( $+1$ ) monopole Weyl nodes, with darker/lighter color variants denoting nodes below/above the Fermi energy, empty circles mark  $\Gamma$ - $X$  double Weyl nodes, and TLTs are marked by circles filled with color corresponding to (a). (b)  $X$ - $W$  regime, (c)  $\Gamma$ - $X$  regime, and (d)  $\Gamma$ - $X$  -  $\Gamma$ - $L$  regime.

The localized electrons are represented by

$$\mathcal{H}_d = E_d \sum_{i,\sigma} d_{i\sigma}^\dagger d_{i\sigma} + U \sum_i n_{i\uparrow}^d n_{i\downarrow}^d + M_z \sum_{i,\sigma} \hat{z} \cdot (d_{i\sigma}^\dagger \boldsymbol{\sigma} d_{i\sigma}), \quad (3)$$

where  $E_d$  is assumed to be much lower in energy than the conduction electron band edge [3], and the Coulomb repulsion  $U$  acts between the  $d$  fermions. The Zeeman interaction with field  $M_z$ , aligned in the  $\hat{z}$  direction, breaks time-reversal symmetry. In a heavy fermion system subjected to a magnetic field, the response of the local moments dominates over orbital effects, so we do not consider Landau levels here.

In the  $U \rightarrow \infty$  (Kondo) limit, the auxiliary boson method is implemented [3], with  $d_{i\sigma} = f_{i\sigma} b_i^\dagger$ . Here, double-occupancy of the  $d$ -electrons is projected out, and small hole-fluctuations away from single-occupation are tracked by the bosonic field,  $b_i \rightarrow \langle b_i \rangle = r$ . The occupation constraint gives rise to a term which takes the place of the Coulomb term,  $\mathcal{H}_\ell = \ell \sum_{i,\sigma} (f_{i\sigma}^\dagger f_{i\sigma} + r^2 - 1)$ . The parameters  $\ell$  and  $r$ , along with  $\mu$ , are determined by solving the system of saddle point equations  $\langle \delta \mathcal{H} / \delta r \rangle = 0$ ,  $\langle \delta \mathcal{H} / \delta \ell \rangle = 0$ , together with the condition for the electron filling. To address the case of a semiconducting conduction-electron background, we consider a total quarter filling  $n_d + n_c = 1$ , which is 1 fermion per site; in the strong coupling limit we have  $n_f + r^2 = 1$ , implying that  $n_c \sim r^2$ . Generically, both the time-reversal and inversion symmetry-breaking will influence the Weyl nodes [24]. We study the extent to which the Kondo-driven Weyl nodal excitations survive the Zeeman coupling and, if they do, whether and how they can be controlled by the magnetic field. A tech-

nique to obtain fast numerical solution convergence is detailed in the Supplemental Material.

**Zeeman-Field Tuning of the Weyl Nodes:** In what follows, we describe several Weyl node configurations in the Brillouin zone (BZ) that we encounter as a function of the Zeeman field, as well as various changes between each WKSM regime. Thus we have chosen to label each WKSM regime by the Weyl node location(s) in the BZ, and the location of the intermediate crossover or critical points between regimes and their dispersion type. The Zeeman field strength is reported as  $M_0 = M_z/T_K^0$ , relative to the Kondo temperature  $T_K^0$ , which is estimated from the bandwidth of the heavy Weyl bands for  $M_z = 0$ , in units of  $\mu_0 = k_B = 1$ ; the parameters held constant are  $\{E_d, V, \lambda, m, t\} = \{-7, 9.29, 0.5, 1, 1\}$ . In Refs. [6, 7], we established the WKSM phase for the time-reversal invariant case, represented by the black starting point of the arrow in the phase diagram of Fig. 1(a): at  $M_0 = 0$ , the nodes can be found along all  $X-W$  lines on the BZ boundary.

When the Zeeman coupling  $M_0$  is small in the yellow-labeled regime, the  $X-W$  nodes *change trajectory* along the yellow arrows in the BZ diagram in Fig. 1(b). With increasing  $M_0$ , the WKSM nodes move throughout the BZ as illustrated in Fig. 1(b)-(d), where we show selected pairs of nodal trajectories whose BZ location and color-coded arrows correspond to the WKSM regimes in Fig. 1(a). The crossover and critical points are denoted by filled circles of corresponding color, at the location in the BZ where they occur. Nodal topological charges are indicated with blue and red dots for  $+1$  and  $-1$ , and empty circles for  $+2$  double Weyl fermions. The darker (lighter) blue and red circles of the  $X-W$  regime indicate that the nodes have moved below (above) the Fermi

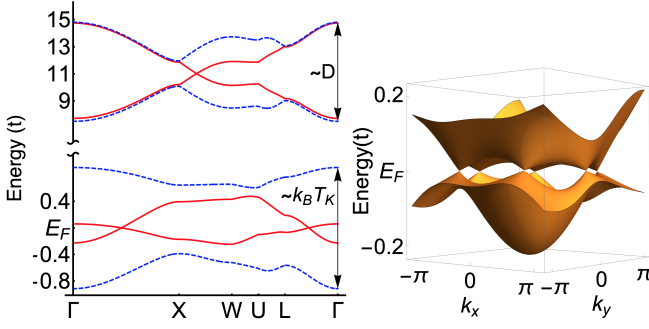


FIG. 2.  $\Gamma$ - $X$  -  $\Gamma$ - $L$  WKSM eigenenergy dispersion at  $M_0 = 0.432$ ; left: high symmetry path through the BZ, right: on the  $[011]$  plane, with origin at  $\Gamma$ . Here,  $D$  is the bare conduction-electron bandwidth.

energy; this occurs only for the  $k_x, k_y = \pm 2\pi$  BZ faces. Correspondingly these off- $E_F$  nodes establish Fermi/hole pockets; these completely disappear in the  $\Gamma$ - $X$ - $\Gamma$ - $L$  regime. Remarkably, all the nodes besides these are pinned to the Fermi energy.

The off-Fermi energy nodes move toward  $W$  until they annihilate with their opposite-charge counterpart in the neighboring BZ in the  $\Gamma$ - $X$  regime; they are accompanied by Fermi/hole pockets that persist into the  $\Gamma$ - $X$ - $\Gamma$ - $L$  regime. The  $k_z = \pm 2\pi$  faces possess nodes that uniformly meet at  $X$ , in contrast to the  $k_x, k_y = \pm 2\pi$  BZ faces; the difference owes to the  $+\hat{z}$  direction of  $M_0$ . At  $M_0 = 0.128$  (yellow circle, Fig. 1(a)), the  $X$ - $W$  nodes indicated in Fig. 1(b) meet at the  $X$  point, where the dispersion forms a non-Kramers' type quadratic band touching, dubbed the  $X$ -QBT point.

When  $0.128 < M_0 < 0.290$ , nodes are formed inside the BZ boundary from the six  $X$  points towards  $\Gamma$  indicated with blue arrows, as shown in Fig. 1(c). In the  $k_x, k_y$ -plane, double Weyl nodes develop along  $\Gamma$ - $X$  with charge  $+2$  [25–34], yet along the  $\hat{z}$ -axis, the Weyl nodes form a monopole charge-opposite pair.

When  $M_0 = 0.290$  (blue circles, Fig. 1(a),(d)), another topological Lifshitz transition occurs, called the  $L$ -ABT point to label an anisotropic band touching at  $L$ : the dispersion along the  $(\pm 1, \pm 1, \pm 1)$  directions has a quadratic band touching, but is linear in the perpendicular plane of the hexagonal BZ boundary. When  $M_0 > 0.290$ , charge  $\pm 1$  Weyl nodes form from the  $L$  points along the  $\Gamma$ - $L$  directions (see Fig. 2). All sets of nodes (3 pairs of  $\Gamma$ - $X$ , 4 pairs of  $\Gamma$ - $L$ ) progress towards  $\Gamma$ , and this  $\Gamma$ - $X$  -  $\Gamma$ - $L$  regime corresponds to the orange regime and arrows in Fig. 1(a),(d).

The normalized Berry curvature field of the  $\Gamma$ - $X$  -  $\Gamma$ - $L$  WKSM is shown in Fig. 3(a), projected onto the  $[011]$  plane to show both the  $\Gamma$ - $X$  and  $\Gamma$ - $L$  nodes. The  $\Gamma$ - $L$  nodes (blue and red points) display sink/source monopole fields, while the  $\Gamma$ - $X$  nodes have field structure for charge  $+2$  double-Weyl fermions [25–31]. In Fig 3(b)-(c), closer field configurations of the  $\Gamma$ - $X$  double Weyl fermions are shown.

**Zeeman-induced Annihilation of the Weyl Nodes:** When the Zeeman coupling approaches the threshold value  $M_0 =$

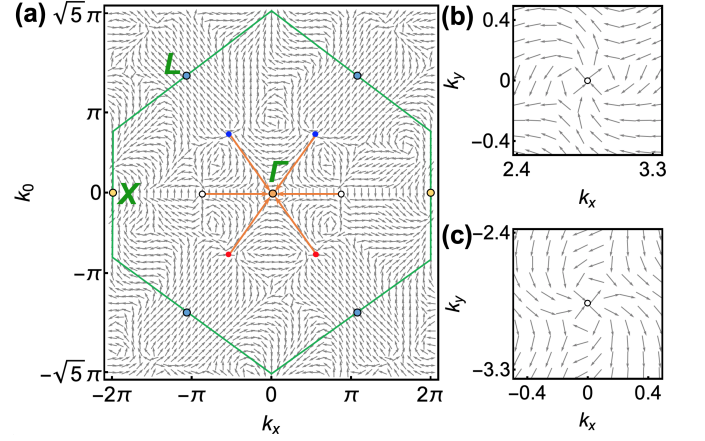


FIG. 3. (a) Berry curvature projected onto the  $[011]$  plane in the  $\Gamma$ - $X$  -  $\Gamma$ - $L$  regime at  $M_0 = 0.432$ . The orange arrows indicate the node pairs' path toward simultaneous annihilation at the  $\Gamma$  point for  $M_0 > 0.432$ . The green line marks the BZ boundary, blue/red (empty) circles mark  $\pm 1$  ( $+2$ ) Weyl nodes, and yellow, blue, and orange circles correspond to the TLT locations of Fig. 1(a).

0.611, all the  $\Gamma$ - $X$  and  $\Gamma$ - $L$  nodes meet in the zone center  $\Gamma$ . This complete annihilation of the Weyl nodes by the Zeeman coupling is illustrated in Fig. 1(d) as well as in Fig. 3(a).

At the threshold coupling  $M_0 = 0.611$ , a quadratic band touching critical point is formed (labeled  $\Gamma$ -QBT) (orange circle, Fig. 4). The  $\Gamma$ -QBT point is non-Kramers (singly degenerate) due to the broken time-reversal symmetry. When  $M_0$  goes beyond this threshold, the  $\Gamma$ -QBT bands open a gap, leading to a KI phase. The emergence of the  $\Gamma$ -QBT point is consistent with a continuous nature of the zero-temperature topological phase transition at this threshold  $M_0$  value.

Indeed,  $\Gamma$ -QBT marks a thermodynamic quantum phase transition that is second order. This is evidenced by the parameters  $\ell$  and  $r$  as a function of  $M_0$  being continuous and showing nonanalyticities (pronounced kinks) across the  $\Gamma$ -QBT point, as seen in Fig. 5.

**Discussion:** Several remarks are in order. First, the WKSM considered here under a Zeeman field produces a WKSM regime with three topologically distinct nodal config-

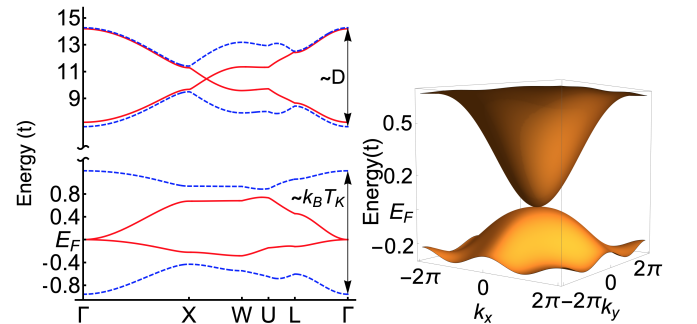


FIG. 4. Eigenenergy dispersion at  $\Gamma$ -QBT; left: high symmetry path through the BZ, right: on the  $k_x$ - $k_y$  plane, with origin at  $\Gamma$ .

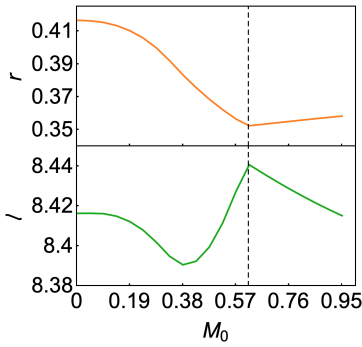


FIG. 5. The saddle-point parameters as a function of  $M_0$ . Top: scalar bosonic condensate  $r$ . Bottom: Lagrange multiplier  $\ell$ . The dashed line marks the kinks at the  $\Gamma$ -QBT point where  $M_0 = 0.611$ .

urations and a phase transition to a Kondo insulator, divided by a non-Kramers quadratic band touching critical point. A large part of the  $M_0$  phase diagram includes double Weyl fermions. It has been suggested in weakly correlated contexts that double Weyl fermions are more sensitive to the effects of interaction and disorder, which could lead to the emergence of a non-Fermi liquid state, and can also produce anomalous screening charge distributions around charged impurities [26]. It was shown that the presence of double Weyl fermions enhance the anomalous Hall effect twofold, and that the Fermi arcs come in pairs [30]. How the underlying strong correlations affect such characteristics in the Zeeman-coupled WKSM, especially in light of the fact that the  $f$ -electron charge response is reduced in the Kondo limit, is an intriguing question to address in the future.

Second, in the weakly correlated Luttinger semimetal  $\alpha$ -Sn with a diamond crystal structure under a magnetic field, a  $k \cdot p$  model reveals double-Weyl nodes at different energies [34]. There, it was found that a linear inversion symmetry breaking term splits the double-Weyl fermions into single-Weyl fermions. By contrast, in our model the double-Weyl fermions are pinned to the Fermi energy, and are present over a range of combined time-reversal and inversion symmetry breaking couplings. The latter reflects the robustness of the Kondo effect that underlies the Weyl nodes.

Third, as the WKSM approaches the thermodynamic and topological quantum phase transition to a KI, the nodes are pinned to the Fermi energy. In the presence of time-reversal symmetry, this effect has been extensively demonstrated. The strong correlation effect underlying the Kondo effect dictates that the Kondo-driven Weyl nodes lie near the Fermi energy within the narrow energy range of the Kondo scale; this effect, when combined with the nonsymmorphic nature of the space group symmetry, pins the Kondo-driven nodes in our model to the Fermi energy [6, 7]. The Zeeman field only reduces the symmetry of the spin degrees of freedom, and so the node-pinning mechanism remains free to operate. The space-group symmetry constraint is a general phenomenon [35–37]. Thus, we expect that the mechanism we have advanced here, for the Zeeman-field-induced WKSM to KI transition, will apply to

Kondo-lattice systems defined on a variety of nonsymmorphic crystalline structures.

Fourth, in lieu of a full phase diagram, we also investigated the zero-field WKSM model as a function of the inversion-symmetry-breaking potential, parameterized by  $m$  [6, 7, 22], without a Zeeman coupling. When  $m = 0$ , inversion symmetry is preserved, and we begin with a Dirac-Kondo semimetal with degeneracies at the  $X$  points. For  $0 < m < 2$ , the inversion-symmetry breaking splits the Dirac cone into four Weyl cones (two monopole pairs) per square BZ boundary, with trajectories from  $X$  to the  $W$  point. At  $m = 2$ , each node meets its opposite charge partner from the neighboring BZ, becoming an anisotropic band touching at  $W$ , before annihilating and forming a gapped state for  $m > 2$ . This transition is similar to the  $\Gamma$ -QBT transition, since the merging of Weyl nodes precipitates their annihilation and gap formation, which in both cases is accompanied by a kink in the saddle-point parameters across the critical point. However, one striking difference is that, in the case of Zeeman tuning at a nonzero  $m$ , the double Weyl nodes emerge, and that the gap opening location occurs at the highly symmetric zone center  $\Gamma$  (which is a time-reversal-invariant momentum) in contrast to annihilation at  $W$ , which is not a time-reversal-invariant momentum and of lower symmetry.

Fifth, our model and its WKSM-KI transition is important to the magnetic field experiments done on the nonmagnetic heavy fermion compound  $\text{Ce}_3\text{Bi}_4\text{Pd}_3$ , where a WKSM-KI transition was observed [20]. The experiments in that work also found a heavy-fermion metal phase at high field values, which is more typical of Kondo-insulator physics, and is not the focus of the present work. What is nontrivial in our finding is that the WKSM phase and its topological Lifshitz transitions take place at a Zeeman field scale smaller than the Kondo scale, before the Kondo effect itself is suppressed by the Zeeman coupling. In that sense, our result captures the most surprising aspect of the experimental findings.

Finally, a Zeeman coupling on the order of the Kondo scale in typical heavy fermion semimetals corresponds to a magnetic field on the order of 10 T. While such a magnetic field would produce a minute Zeeman effect in non-interacting semimetals, for WKSMs it is enough to modify the Weyl nodes in a drastic way. This captures the correlation-enhanced responses of the WKSM. We expect that this feature also applies to related models based on Kondo effects [38–43], as well as to other materials, such as  $\text{CeRu}_4\text{Sn}_6$  [44–49],  $\text{Yb-BiPt}$  [50–53] and  $\text{CeSbTe}$  [54], which are considered to be WKSM candidates.

**Summary:** This work has addressed the effect of Zeeman coupling in a nonsymmorphic and noncentrosymmetric Kondo lattice model, in which the cooperation of the Kondo effect and space-group symmetry produces Weyl nodes near the Fermi energy. We have demonstrated an extreme responsiveness of the Weyl nodes to the Zeeman coupling. Several topologically-distinct semimetal regimes are induced by the Zeeman coupling, which involve double Weyl points that may significantly affect the anomalous magnetotransport proper-

ties. We have shown that a Zeeman coupling that is smaller than the zero-field Kondo energy scale is adequate to fully annihilate all the Weyl nodes, leading to a second-order topological quantum phase transition to a Kondo insulator. This result is important for understanding the recent high magnetic-field experiments in  $\text{Ce}_3\text{Bi}_4\text{Pd}_3$ . More generally, our findings show how strong correlations and space-group symmetry cooperate to produce correlation-elevated control of topological excitations. This illustrates how strongly correlated topological systems may provide new platforms for quantum applications.

We thank Pallab Goswami, Sami Dzsaber, Jennifer Cano, Diego Zocco, Mathieu Taupin for useful discussions. Work at Rice has been supported by the NSF (DMR-1920740), the Robert A. Welch Foundation (C-1411) and the ARO (W911NF-14-1-0525). Work at Los Alamos was carried out under the auspices of the U.S. Department of Energy (DOE) National Nuclear Security Administration under Contract No. 89233218CNA000001, and was supported by LANL LDRD Program. Work in Vienna was supported by the Austrian Science Fund (projects P29279 and P29296) and the European Community (H2020 project 824109).

---

\* seg@lanl.gov

- [1] B. Keimer and J. E. Moore, *Nature Physics* **13**, 1045 (2017).
- [2] S. Paschen and Q. Si, *Nature Reviews Physics* (2020), 10.1038/s42254-020-00262-6.
- [3] A. C. Hewson, *The Kondo Problem to Heavy Fermions* (Cambridge University Press, 2003).
- [4] S. Kirchner, S. Paschen, Q. Chen, S. Wirth, D. Feng, J. D. Thompson, and Q. Si, *Rev. Mod. Phys.* **92**, 011002 (2020).
- [5] H. v. Löhneysen, A. Rosch, M. Vojta, and P. Wölfle, *Rev. Mod. Phys.* **79**, 1015 (2007).
- [6] H.-H. Lai, S. E. Grefe, S. Paschen, and Q. Si, *Proceedings of the National Academy of Sciences* **115**, 93 (2018).
- [7] S. E. Grefe, H.-H. Lai, S. Paschen, and Q. Si, *Phys. Rev. B* **101**, 075138 (2020).
- [8] S. Dzsaber, L. Prochaska, A. Sidorenko, G. Eguchi, R. Svagera, M. Waas, A. Prokofiev, Q. Si, and S. Paschen, *Phys. Rev. Lett.* **118**, 246601 (2017).
- [9] S. Dzsaber, X. Yan, M. Taupin, G. Eguchi, A. Prokofiev, T. Shiroka, P. Blaha, O. Rubel, S. E. Grefe, H.-H. Lai, Q. Si, and S. Paschen, “Giant spontaneous Hall effect in a nonmagnetic Weyl-Kondo semimetal,” (2018), arXiv:1811.02819 [cond-mat.str-el].
- [10] K. Heuser, E.-W. Scheidt, T. Schreiner, and G. R. Stewart, *Phys. Rev. B* **57**, R4198 (1998).
- [11] S. Paschen, T. Lühmann, S. Wirth, P. Gegenwart, O. Trovarelli, C. Geibel, F. Steglich, P. Coleman, and Q. Si, *Nature* **432**, 881 (2004).
- [12] S. Nair, S. Wirth, S. Friedemann, F. Steglich, Q. Si, and A. J. Schofield, *Advances in Physics* **61**, 583 (2012), <https://doi.org/10.1080/00018732.2012.730223>.
- [13] Q. Si and S. Paschen, *Physica Stat. Solidi B* **250**, 425 (2013).
- [14] H. Shishido, R. Settai, H. Harima, and Y. Onuki, *J. Phys. Soc. Jpn.* **74**, 1103 (2005).
- [15] T. Park, F. Ronning, H. Q. Yuan, M. B. Salamon, R. Movshovich, J. L. Sarrao, and J. D. Thompson, *Nature* **440**, 65 (2006).
- [16] G. Knebel, D. Aoki, J.-P. Brison, and J. Flouquet, *J. Phys. Soc. Jpn.* **77**, 114704 (2008).
- [17] Q. Si, S. Rabello, K. Ingersent, and J. L. Smith, *Nature* **413**, 804 (2001).
- [18] P. Coleman, C. Pépin, Q. Si, and R. Ramazashvili, *Journal of Physics: Condensed Matter* **13**, R723 (2001).
- [19] Q. Si, *Physica B: Condensed Matter* **378-380**, 23 (2006).
- [20] S. Dzsaber, D. A. Zocco, A. McCollam, F. Weickert, R. McDonald, M. Taupin, X. Yan, A. Prokofiev, L. M. K. Tang, B. Vlaar, L. Stritzinger, M. Jaime, Q. Si, and S. Paschen, “Quenching a Weyl-Kondo semimetal by magnetic field,” (2019), arXiv:1906.01182 [cond-mat.str-el].
- [21] L. Fu, C. L. Kane, and E. J. Mele, *Phys. Rev. Lett.* **98**, 106803 (2007).
- [22] T. Ojanen, *Phys. Rev. B* **87**, 245112 (2013).
- [23] S. Murakami and S.-i. Kuga, *Phys. Rev. B* **78**, 165313 (2008).
- [24] S. E. Grefe, H.-H. Lai, S. Paschen, and Q. Si, *Proceedings of the International Conference on Strongly Correlated Electron Systems (SCES2019)*, JPS Conference Proceedings **30**, 011013 (2020).
- [25] C. Fang, M. J. Gilbert, X. Dai, and B. A. Bernevig, *Phys. Rev. Lett.* **108**, 266802 (2012).
- [26] B.-J. Yang and N. Nagaosa, *Nature Communications* **5**, 4898 (2014).
- [27] S.-K. Jian and H. Yao, *Phys. Rev. B* **92**, 045121 (2015).
- [28] X. Li, B. Roy, and S. Das Sarma, *Phys. Rev. B* **94**, 195144 (2016).
- [29] S.-M. Huang, S.-Y. Xu, I. Belopolski, C.-C. Lee, G. Chang, T.-R. Chang, B. Wang, N. Alidoust, G. Bian, M. Neupane, D. Sanchez, H. Zheng, H.-T. Jeng, A. Bansil, T. Neupert, H. Lin, and M. Z. Hasan, *Proceedings of the National Academy of Sciences* **113**, 1180 (2016), <https://www.pnas.org/content/113/5/1180.full.pdf>.
- [30] M. Ezawa, *Phys. Rev. B* **96**, 161202 (2017).
- [31] M. Ezawa, *Phys. Rev. B* **96**, 041205 (2017).
- [32] S. Ahn, E. J. Mele, and H. Min, *Phys. Rev. B* **95**, 161112 (2017).
- [33] Z. Yan and Z. Wang, *Phys. Rev. B* **96**, 041206 (2017).
- [34] D. Zhang, H. Wang, J. Ruan, G. Yao, and H. Zhang, *Phys. Rev. B* **97**, 195139 (2018).
- [35] J. Cano, B. Bradlyn, Z. Wang, L. Elcoro, M. G. Vergniory, C. Felser, M. I. Aroyo, and B. A. Bernevig, *Phys. Rev. B* **97**, 035139 (2018).
- [36] H. Watanabe, H. C. Po, M. P. Zaletel, and A. Vishwanath, *Phys. Rev. Lett.* **117**, 096404 (2016).
- [37] S. M. Young, S. Zaheer, J. C. Y. Teo, C. L. Kane, E. J. Mele, and A. M. Rappe, *Phys. Rev. Lett.* **108**, 140405 (2012).
- [38] X.-Y. Feng, J. Dai, C.-H. Chung, and Q. Si, *Phys. Rev. Lett.* **111**, 016402 (2013).
- [39] X.-Y. Feng, H. Zhong, J. Dai, and Q. Si, “Dirac-Kondo semimetals and topological Kondo insulators in the dilute carrier limit,” (2016), arXiv:1605.02380 [cond-mat.str-el].
- [40] S. Ok, M. Legner, T. Neupert, and A. M. Cook, “Magnetic Weyl and Dirac Kondo semimetal phases in heterostructures,” (2017), arXiv:1703.03804 [cond-mat.str-el].
- [41] P.-Y. Chang and P. Coleman, *Phys. Rev. B* **97**, 155134 (2018).
- [42] J. H. Pixley, S. B. Lee, B. Brandom, and S. A. Parameswaran, *Phys. Rev. B* **96**, 081105(R) (2017).
- [43] C. Cao, G.-X. Zhi, and J.-X. Zhu, *Phys. Rev. Lett.* **124**, 166403 (2020).
- [44] W. T. Fuhrman, A. Sidorenko, J. Hänel, H. Winkler, A. Prokofiev, J. A. Rodriguez-Rivera, Y. Qiu, P. Blaha, Q. Si, C. L. Broholm, and S. Paschen, “Pristine quantum criticality in

- a kondo semimetal,” (2020), arXiv:2007.09460 [cond-mat.str-el].
- [45] S. Paschen, H. Winkler, T. Nezu, M. Kriegisch, G. Hilscher, J. Custers, A. Prokofiev, and A. Strydom, *Journal of Physics: Conference Series* **200**, 012156 (2010).
  - [46] V. Guritanu, P. Wissgott, T. Weig, H. Winkler, J. Sichelschmidt, M. Scheffler, A. Prokofiev, S. Kimura, T. Iizuka, A. M. Strydom, M. Dressel, F. Steglich, K. Held, and S. Paschen, *Phys. Rev. B* **87**, 115129 (2013).
  - [47] M. Sundermann, F. Strigari, T. Willers, H. Winkler, A. Prokofiev, J. M. Ablett, J.-P. Rueff, D. Schmitz, E. Weschke, M. M. Sala, A. Al-Zein, A. Tanaka, M. W. Haverkort, D. Kasinathan, L. H. Tjeng, S. Paschen, and A. Severing, *Scientific Reports* **5**, 17937 (2015).
  - [48] P. Wissgott and K. Held, *The European Physical Journal B* **89**, 5 (2016).
  - [49] Y. Xu, C. Yue, H. Weng, and X. Dai, *Phys. Rev. X* **7**, 011027 (2017).
  - [50] C. Y. Guo, F. Wu, Z. Z. Wu, M. Smidman, C. Cao, A. Bostwick, C. Jozwiak, E. Rotenberg, Y. Liu, F. Steglich, and H. Q. Yuan, *Nature Communications* **9**, 4622 (2018).
  - [51] Z. Fisk, P. C. Canfield, W. P. Beyermann, J. D. Thompson, M. F. Hundley, H. R. Ott, E. Felder, M. B. Maple, M. A. Lopez de la Torre, P. Visani, and C. L. Seaman, *Phys. Rev. Lett.* **67**, 3310 (1991).
  - [52] S. Chadov, X. Qi, J. Kübler, G. H. Fecher, C. Felser, and S. C. Zhang, *Nature Materials* **9**, 541 (2010).
  - [53] E. D. Mun, S. L. Bud’ko, C. Martin, H. Kim, M. A. Tanatar, J.-H. Park, T. Murphy, G. M. Schmiedeshoff, N. Dilley, R. Prozorov, and P. C. Canfield, *Phys. Rev. B* **87**, 075120 (2013).
  - [54] L. M. Schoop, A. Topp, J. Lippmann, F. Orlandi, L. Mühler, M. G. Vergniory, Y. Sun, A. W. Rost, V. Duppel, M. Krivenkov, S. Sheoran, P. Manuel, A. Varykhalov, B. Yan, R. K. Kremer, C. R. Ast, and B. V. Lotsch, *Science Advances* **4**, eaar2317 (2018).